J Mater Sci (2007) 42:4009–4017
DOI 10.1007/s10853-006-0236-z

# Improved visible-light responsive photocatalytic activity of N and Si co-doped titanias

**Hirotaka Ozaki · Shinji Iwamoto · Masashi Inoue**

Received: 6 February 2006 / Accepted: 13 April 2006 / Published online: 31 January 2007


**Abstract** Thermal reaction of titanium tetraisopropoxide and tetraethyl orthosilicate in 1,4-butanediol afforded nanocrystalline silica-modified titanias having large surface area and superior thermal stability. In this study, the thus-obtained silica-modified titanias were treated in an $NH_3$ flow at high temperatures, and their physical and photocatalytic properties were investigated. Compared with $NH_3$-treated $TiO_2$ without silica modification, the $NH_3$-treated silica-modified titanias showed a stronger absorption in the visible region (400–500 nm) and had a larger peak at 396 eV in the N 1s XPS spectrum. These results indicate that a larger amount of nitrogen was stably doped in the silica-modified titania. The obtained products exhibited a high photocatalytic activity for degradation of Rhodamine B and decomposition of acetaldehyde under visible light irradiation.

## Introduction

The photocatalytic and photoelectrochemical applications of semiconductor materials have attracted great attention. Among various photocatalyst materials, titanium dioxide ($TiO_2$) has been most widely used and investigated [1, 2], because it has advantages in inexpensiveness, chemical stability, and nontoxicity in addition to its favorable optoelectronic property. However, the band gap of anatase $TiO_2$ is 3.2 eV; therefore, the photocatalytic reaction proceeds only by irradiation of ultraviolet (UV) light (wavelength ($\lambda$) < 388 nm), which means only about 3% of the incoming solar energy on the earth's surface can be utilized.

In recent years, a number of attempts have been made to expand the photosensitivity of $TiO_2$-based photocatalysts into the visible light region. One approach is introduction of allowed energy states in the band gap of $TiO_2$ by doping of transition metal cations such as Cr, V or Fe [3–6]. However, the introduction of these cations causes an increase in the population of recombination centers, which usually results in a low photoefficiency. Another approach is use of anionic species, such as C, N, F and S [7–13]. Nitrogen-doped $TiO_2$ materials were reported by Sato for the first time in 1986 [7]. He found that the calcination of $Ti(OH)_4$ involving ammonium compounds gave yellowish powders that exhibited photocatalytic activities under visible light irradiation. Recently, several groups also reported the visible light sensitivity of N-doped $TiO_2$ materials [8–10] Asahi et al. [8] reported that nitrogen-doped $TiO_2$ thin films showed photocatalytic activities under visible light irradiation. They reported that the visible light sensitivity of the nitrogen-doped $TiO_2$ was due to the narrowing of the energy gap by mixing N 2p and O 2p states. Lindgren et al. [9] prepared nanocrystalline porous nitrogen-doped $TiO_2$ films by the DC magnetron sputtering method and examined their photoelectrochemical properties. It was reported that although all the nitrogen-doped films showed visible light absorption in the

**Electronic supplementary material** The online version of this article (doi:10.1007/s10853-006-0236-z) contains supplementary material, which is available to authorized users.

H. Ozaki · S. Iwamoto (✉) · M. Inoue
Department of Energy and Hydrocarbon Chemistry, Graduate School of Engineering, Kyoto University, Katsura, Kyoto 615-8510, Japan
e-mail: iwamoto@scl.kyoto-u.ac.jp

wavelength range from 400 to 535 nm, there was an optimum concentration of nitrogen where the response was highest. Irie et al. compared quantum yields in the photocatalytic decomposition of 2-propanol using $TiO_xN_y$ powders. They found that the highest quantum yield was obtained for a sample with a very low concentration of nitrogen, the N/Ti ratio of 0.005, and that further increase in the nitrogen concentration lowered the quantum yield due to the increase in the recombination rate [10]. Although these reports showed that nitrogen-doping is an effective method to induce a visible light sensitivity to $TiO_2$, they also suggested that in the ternary Ti–O–N system, an improvement of the photoefficiency under visible light irradiation is difficult.

We previously reported that the thermal reactions of titanium tetraisopropoxide and tetraethyl orthosilicate in 1,4-butanediol (glycothermal reaction) afforded nanocrystalline silica-modified titanias with the anatase structure having large surface areas and superior thermal stabilities [14]. The obtained silica-modified titanias were characterized by XPS and XANES, and it was found that the Si atoms are inserted in the distorted octahedral vacant sites of the anatase structure [15]. Such insertion of the Si atoms causes unbalanced positive charges. We observed that the concentration of the surface OH groups decreased by the silica modification. These two results are reasonably explained as follows: substitution of the surface OH groups with surface oxide ions forms negative charge which compensates for the positive charge caused by the insertion of the Si in the vacant sites. From the obtained results, we expect that substitution of $O^{2-}$ with $N^{3-}$ in the silica-modified titanias would take place more easily because such additional negative charge cancels the extra positive charge caused by the Si incorporation. We examined, accordingly, the nitrification of the silica-modified titanias and found that the titanias co-doped with Si and N showed a strong absorption in the visible region (400–500 nm) and exhibited high photocatalytic activities for degradation of RhB and decomposition of acetaldehyde under visible light irradiation. Recently, we published a preliminary report of our findings [16]. In the present paper, we show the physical properties and the photocatalytic activities of N and Si co-doped titania in detail.

## Experimental

Titania and silica-modified titania were prepared by the glycothermal method and collected as a xerogel form [17]: titanium tetraisopropoxide (25 g) and an appropriate amount of tetraethyl orthosilicate (Si/Ti atomic ratio of 0 or 0.1) were added to 100 mL of 1,4-butanediol and this mixture was placed in a 300 mL autoclave equipped with two valves, one of which was used as a gas inlet and the other was connected to a Liebig condenser of stainless tubing. After the atmosphere inside the autoclave was replaced with nitrogen, the assembly was heated to 300 °C at a rate of 2.3 °C/min and kept at that temperature for 2 h. After the glycothermal reaction, the valve of the autoclave was slightly opened in order to remove the organic vapor from the autoclave by flash evaporation while keeping the autoclave temperature at 300 °C. After cooling, bulky solid products were directly obtained. The product was calcined in a box furnace in air at 500 °C for 30 min to remove the surface organic moieties. The thus-obtained products are designated as XG(x), where x is the Si/Ti charged ratio. XG(x) was placed in a quartz tube reactor, heated to a desired temperature (450–700 °C) at a rate of about 10 °C/min in a 100 mL/min flow of argon, and allowed to react in an $NH_3$ flow (100 mL/min) for 1 h, 3 h or 5 h at that temperature. After the $NH_3$ treatment, the sample was annealed at 400 °C in air for 30 min using a box furnace in order to eliminate the adsorbed $NH_3$ on the catalyst. JRC-TIO-4 (a reference catalyst supplied from The Catalysis Society of Japan; equivalent to Degussa P-25; rutile/anatase = 3/7; BET surface area = 49 $m^2/g$) was nitrified in the same way.

The UV–vis absorption spectra were recorded on a Shimadzu MPS-2000 spectrophotometer. Powder X-ray diffraction (XRD) patterns were recorded on a Shimadzu XD-D1 diffractometer using CuKα radiation and a carbon-monochromator. The specific surface areas of the samples were determined by the BET single-point method on the basis of the nitrogen uptake measured at 77 K using a Micromeritics Flowsorb II 2300. X-ray photoelectron spectroscopy (XPS) measurement was performed on an ULVAC-PHI Model 5500 spectrometer with 15 kV–400 W MgKα emission as the X-ray source. The zeta potentials were measured on an electrophoretic light scattering spectrophotometer, Otsuka Electronics, ELS-800.

Photocatalytic activity was evaluated by degradation of Rhodamine B (RhB) and decomposition of acetaldehyde. As for the RhB degradation, 20 mg of the catalyst was dispersed in 100 mL of $1.0 \times 10^{-5}$ mol/L RhB solution and the obtained suspension was irradiated with blue-light-emitting diodes (blue LED, NSPB510S, Nichia). The blue LED has an emission wavelength ranging from 420 to 520 nm and a peak wavelength at 470 nm. The power of a blue LED device used in this study was 72 mW, and 96 pieces of the devices were used as a light source (4 panels equipped with 24 devices). After a certain period of

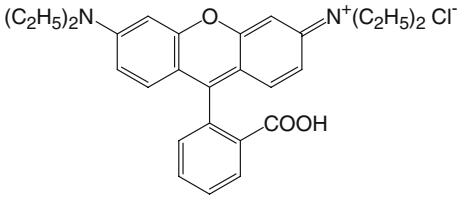


Rhodamine B (RhB)

irradiation, a portion of the suspension was taken out to measure the concentration of the remaining RhB by using the UV–vis spectrometer.

The decomposition of acetaldehyde was carried out in a closed glass reaction vessel (1.0 L). The catalyst (0.2 g) dispersed on a 90 mm∅ glass filter was placed in the vessel and 0.2 mmol acetaldehyde was injected in it. The vessel was placed in the dark for 1 h and then visible light was irradiated using a 300 W xenon lamp (Optical Modulex SX-UI300XQ, Ushio Inc.) through a UV cut-off filter (L-42, Asahi Technoglass Co. Ltd.) and an infrared cut-off filter (Super Cold Filter, Ushio Inc.). After a certain period of irradiation, the $CO_2$ concentration was measured by a gas chromatograph, Shimadzu GC-8A. The amount of $CO_2$ formed was calculated by subtracting the initial amount of $CO_2$ in the vessel.

## Results and discussion

### Physical properties of XG(x)'s after $NH_3$ treatment

White powders of the mother $TiO_2$, XG(0), turned into gray, dark blue and black by the $NH_3$ treatment at 600 °C, 650 °C and 700 °C, respectively, while the colors of $NH_3$-treated XG(0.1) were yellow, yellowish-green and dark blue, respectively. Those colors indicated the samples were nitrified by the $NH_3$ treatment. When the samples were taken out from the reactor after the $NH_3$ treatment and exposed to air, a slight decolorization was observed, which indicates that these $NH_3$-treated samples were partly oxidized in air at room temperature. Figure 1 shows the UV–vis absorption spectra of $NH_3$-treated XG(0)'s. Whereas untreated XG(0) exhibited an absorption only in the UV region (<400 nm), the sample treated at 450 °C in an $NH_3$ flow showed absorption bands at the visible light region (>400 nm). The absorbance at the visible light region gradually became stronger as the $NH_3$ treatment temperature increased to 600 °C, and the absorbance abruptly increased at 650 °C. Similar results were

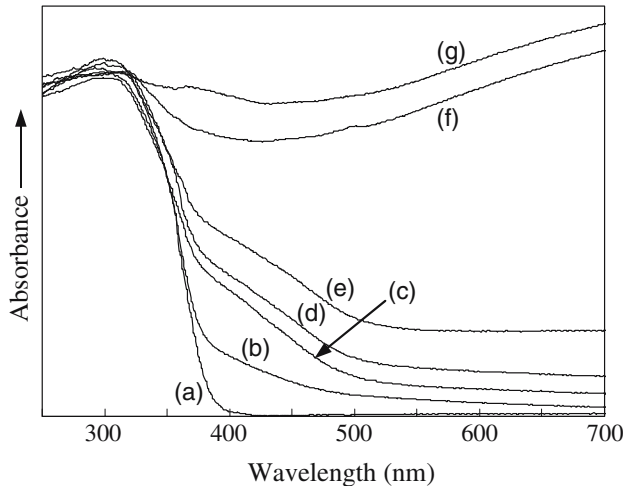


**Fig. 1** UV–vis spectra of XG(0)'s (a), without $NH_3$ treatment; treated in an $NH_3$ flow at: (b), 450 °C; (c), 500 °C; (d), 550 °C; (e), 600 °C; (f), 650 °C; (g), 700 °C; for 1 h

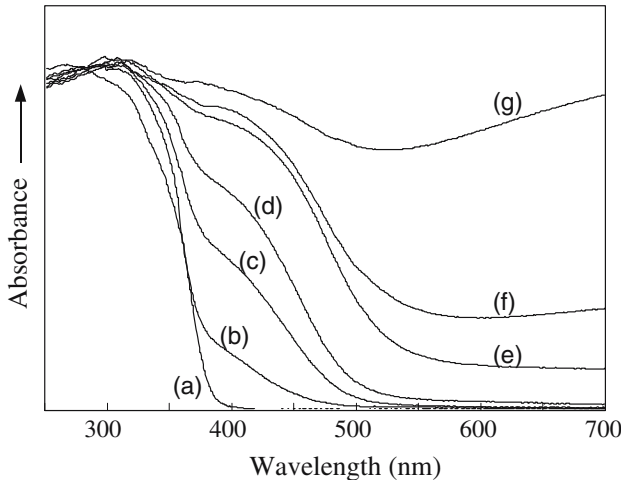


**Fig. 2** UV–vis spectra of XG(0.1)'s (a), without $NH_3$ treatment; treated in an $NH_3$ flow at: (b), 450 °C; (c), 500 °C; (d), 550 °C; (e), 600 °C; (f), 650 °C; (g), 700 °C; for 1 h

reported by several authors [10, 18–20]. The spectra of the $NH_3$-treated samples had a shoulder absorption band at 400–500 nm and a broad band at higher wavelength (>500 nm). The former band is attributed to the doped nitrogen into the anatase structure and the latter corresponds to the formation of $Ti^{3+}$ [21].

Figure 2 shows the absorption spectra of the silica-modified titanias, XG(0.1)'s, heated in an $NH_3$ flow. As compared with the spectra of $NH_3$-treated XG(0) shown in Fig. 1, $NH_3$-treated XG(0.1) have a stronger absorption at 400–500 nm. This result clearly indicates that larger amounts of nitrogen were doped in XG(0.1)'s than in XG(0)'s. On the other hand, at

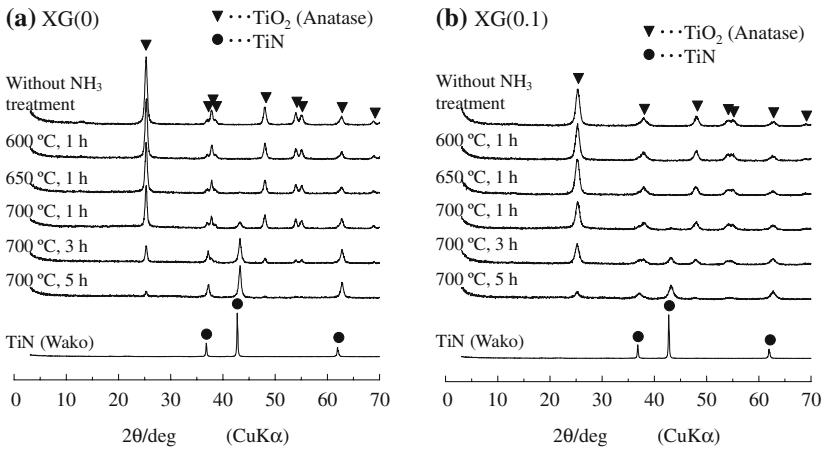


**Fig. 3** XRD patterns of (**a**) XG(0)'s and (**b**) XG(0.1)'s

higher wavelength, the absorptions in XG(0.1)'s were very weak compared with those of XG(0)'s, indicating the reduction of $Ti^{4+}$ to $Ti^{3+}$ was significantly suppressed by the silica modification.

The XRD patterns of the samples are shown in Fig. 3. Both XG(0) and XG(0.1) were composed of anatase nanocrystals and their crystallite sizes were 18 nm and 10 nm, respectively. After the $NH_3$ treatment at 600 °C for 1 h, the samples preserved the anatase structure. For XG(0) treated at 650 °C, a small diffraction peak appeared at $2\theta = 43°$ besides the peaks due to anatase. The sample treated at 700 °C exhibited three peaks at 37°, 43° and 63° and the intensities of the peaks increased with prolonging the treatment time. The diffraction pattern suggests the formation of a rock salt structure, isomorphous to TiN, but the peaks of the samples treated in $NH_3$ at 700 °C were observed at higher diffraction angles than those observed for a reference TiN specimen (Wako chemicals). The lattice parameter was 0.418 nm for both XG(0) and XG(0.1) treated in $NH_3$ at 700 °C for 5 h and that of TiN (Wako) was 0.424 nm. Guillot et al. [22] reported that thin films of $TiN_xO_y$ deposited by DC magnetron sputtering had the rock salt structure and its lattice parameter was 0.422 nm, which is smaller than that of pure TiN. Makino et al. [23] also reported that the lattice constant of titanium oxynitride films produced by the arc ion plating method decreased when the content of oxygen in the compounds increased. Therefore, the newly appeared peaks were assigned to a $TiN_xO_y$ phase, which is designated as $TiN_xO_y$(rock-salt) hereafter. For XG(0.1), the diffraction peaks for $TiN_xO_y$(rock-salt) were not observed after the $NH_3$ treatment at 650 °C or lower temperatures. Treatment at 700 °C gave the peaks but their intensities were much lower than those of XG(0), indicating that the silica-modification suppressed the formation of $TiN_xO_y$(rock-salt).

**Table 1** Physical properties of XG(x)'s treated in an $NH_3$ flow at various temperatures for 1 h and annealed in air at 400 °C for 30 min

| Sample | $NH_3$ treatment temperature (°C) | BET surface area ($m^2/g$) | Crystallite size (nm) | Color |
|---|---|---|---|---|
| XG(0) | | 81 | 18 | White |
| | 500 | 77 | 18 | Pale gray |
| | 600 | 70 | 21 | Gray |
| | 700 | 60 | 25 | Pale brown |
| XG(0.1) | | 152 | 10 | White |
| | 500 | 145 | 10 | Pale yellow |
| | 600 | 149 | 10 | Yellow |
| | 700 | 142 | 11 | Orange |

## Physical properties of $NH_3$-treated and annealed XG(x)'s

The BET surface areas, the crystallite sizes and the colors of $NH_3$-treated XG(x)'s after annealing are summarized in Table 1. XG(0.1) had a smaller crystallite size and a larger surface area than those of XG(0). Even after the $NH_3$ treatment and annealing, the crystallite sizes and BET surface areas of XG(0.1) did not change significantly, indicating that XG(0.1) had a superior thermal stability as compared to XG(0). The annealing treatment caused a decolorization; for example, black color of XG(0) after the $NH_3$ treatment at 700 °C turned into pale brown, and dark blue of XG(0.1) became orange. These results indicate that the annealing at 400 °C resulted in not only the desorption of the adsorbed $NH_3$ from the surface but also the denitrification from the bulk of the samples.

Figure 4 shows the UV–vis absorption spectra of nitrified XG(0) with annealing treatment at 400 °C. Compared with the spectra before annealing shown in Fig. 1, the absorption in the visible light region

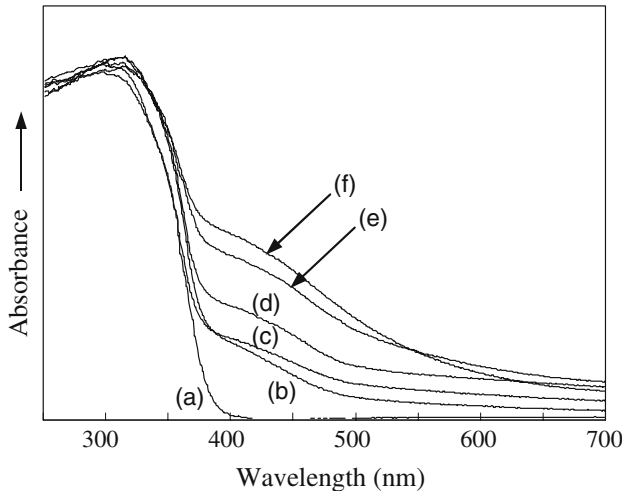


**Fig. 4** UV–vis spectra of XG(0)'s (a), without $NH_3$ treatment; treated in an $NH_3$ flow at: (b), 500 °C; (c), 550 °C; (d), 600 °C; (e), 650 °C; (f), 700 °C; for 1 h and annealed in air at 400 °C for 30 min

decreased, indicating the decrease in the amounts of both the doped nitrogen and the $Ti^{3+}$. Especially, in the case of XG(0) $NH_3$-treated at higher temperatures (650 and 700 °C), the absorption decreased significantly. After the annealing in air at 400 °C, the XRD patterns of the samples showed only peaks due to the anatase structure. These results suggest that the $TiN_xO_y$(rock-salt) phase is not stable under the oxidative conditions at high temperatures. For XG(0), the broad absorption at higher wavelength did not disappear completely, indicating that a certain amount of $Ti^{3+}$ remained in the samples.

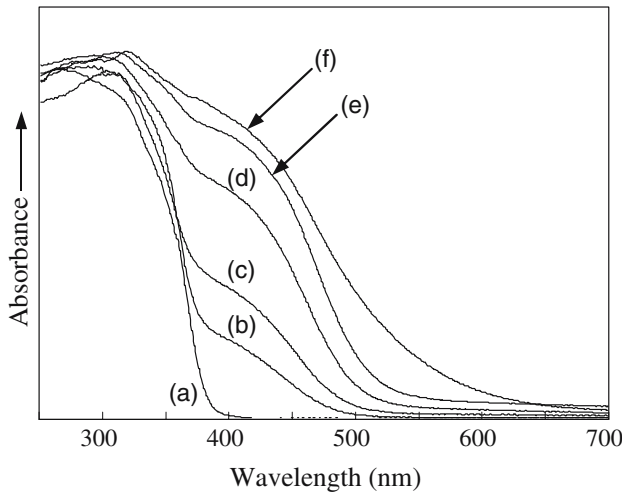


**Fig. 5** UV–vis spectra of XG(0.1)'s (a), without $NH_3$ treatment; treated in an $NH_3$ flow at: (b), 500 °C; (c), 550 °C; (d), 600 °C; (e), 650 °C; (f), 700 °C; for 1 h and annealed in air at 400 °C for 30 min

Figure 5 shows the UV–vis absorption spectra of annealed XG(0.1). On the contrary to the results for XG(0), the absorbance at the higher wavelength region was apparently lower and the shoulder band at 400–500 nm was much stronger. These results indicate that the formation of $Ti^{3+}$ was effectively suppressed, while nitrogen was stably doped in the silica-modified titania.

## XPS studies of nitrified XG(x)'s

In Fig. 6, the N 1s XPS spectra of the samples are depicted. The N 1s XPS spectrum of XG(0) (or XG(0.1); data not shown) without the $NH_3$ treatment exhibited a peak at 400 eV binding energy (BE), which is due to nitrogen-containing species adsorbed on the surface [24]. After the $NH_3$ treatment at 600 °C for 1 h, another peak appeared at 396 eV BE, which is assigned to nitrogen doped in $TiO_2$ [25]. The binding energy of this peak, 396 eV, is much lower than the N 1s BE of nitrogen containing species which are observed at around 400 eV [26], and is close to that of nitrides, 397 eV in TiN [27, 28]. Therefore, the peak at 396 eV is assigned as a nitrogen with a negative charge that substitute oxygen in the lattice position. The intensity of the peak at 396 eV BE in $NH_3$-treated XG(0.1) was obviously larger than that of $NH_3$-treated

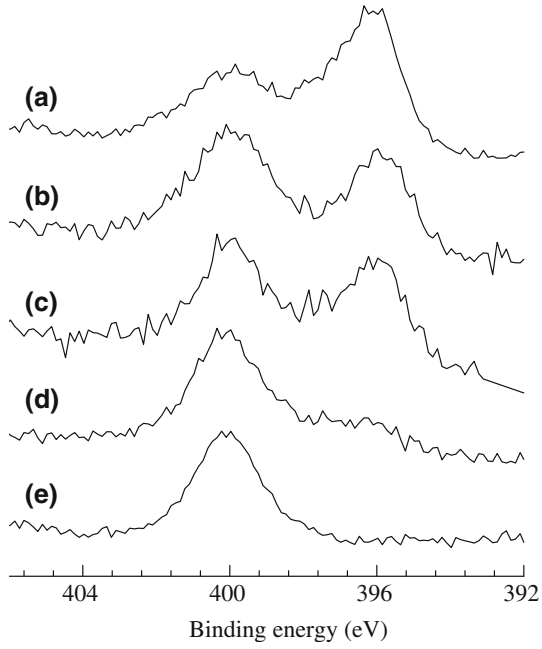


**Fig. 6** N 1s XPS spectra of (a), XG(0.1); (c), XG(0); treated in an $NH_3$ flow at 600 °C for 1 h; (b), XG(0.1); (d), XG(0); after the $NH_3$ treatment followed by annealing at 400 °C for 30 min; and (e), XG(0) without $NH_3$ treatment

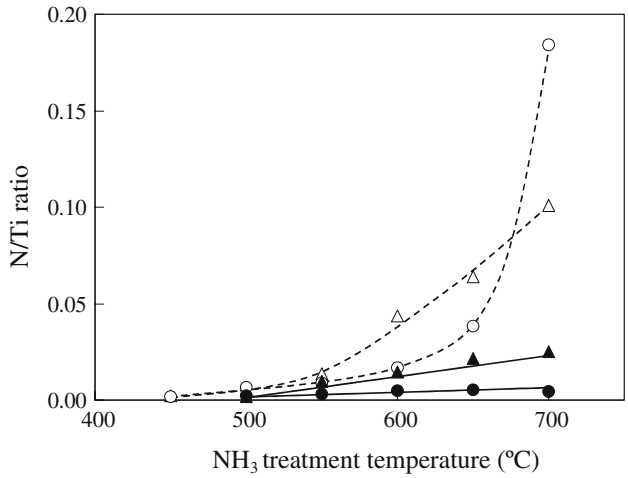


**Fig. 7** N/Ti ratios of the nitrified samples determined by XPS (△) and (▲), for XG(0.1); (○) and (●), for XG(0). Open symbols, after $NH_3$ treatment; solid symbols, after $NH_3$ treatment followed by annealing at 400 °C in air for 30 min

XG(0). Although the intensity of the peak at 396 eV BE decreased in both XG(0) and XG(0.1) after annealing in air at 400 °C for 30 min, the peak at 396 eV BE was clearly observed in the spectrum of XG(0.1). The N/Ti ratios calculated from the intensities of the Ti and $N_{396\,eV}$ peaks are plotted as a function of the $NH_3$ treatment temperature (Fig. 7).

The N/Ti ratios increased with an increase in the treatment temperature. The N/Ti ratios of $NH_3$-treated XG(0.1) were higher than those of $NH_3$-treated XG(0) at temperature up to 650 °C. However, at 700 °C the N/Ti ratio of $NH_3$-treated XG(0) abruptly increased and became higher than that of $NH_3$-treated XG(0.1). This enhancement is due to the formation of $TiN_xO_y$(rock-salt), as was observed by XRD. After annealing at 400 °C, the N/Ti ratios decreased significantly in both XG(0) and XG(0.1). Here, it should be emphasized that the N/Ti ratios of nitrified XG(0.1) were several times higher than those of nitrified XG(0), suggesting that nitrogen atoms were more stably doped in silica-modified titanias than in titania, XG(0). In the silica-modified titanias, silicon atoms are inserted in the distorted octahedral vacant sites in the anatase structure, which caused unbalanced positive charge in the particles [15]. On the other hand, the substitution of $O^{2-}$ with $N^{3-}$ gave excess negative charge. In the case of nitrified silica-modified titanias, the positive charge formed by the Si insertion is compensated by the negative charge by the substitution of $O^{2-}$ with $N^{3-}$. This explains the more stable doping of nitrogen in the silica-modified titanias than in titanias.

The Ti 2p XPS spectra of the samples are shown in Fig. 8. The results for the deconvolution of the Ti 2p peaks are summarized in Table 2. The Ti $2p_{1/2}$ and the Ti $2p_{3/2}$ binding energies of XG(x)'s without the $NH_3$ treatment were about 464.5 eV and 458.8 eV, respectively. After the $NH_3$ treatment at 600 or 650 °C, the Ti 2p XPS spectra did not change significantly. For XG(x)'s with the $NH_3$ treatment at 700 °C for 1 h, however, different components were observed at around 461.8 and 456.1 eV for Ti $2p_{1/2}$ and Ti $2p_{3/2}$, respectively. These components are attributed to titanium in $TiN_xO_y$(rock-salt) [29, 30]. The intensity of the newly observed peak in XG(0.1) treated in $NH_3$ at 700 °C for 1 h was obviously lower than that in XG(0) treated at 700 °C for 1 h. This result indicates that the formation of $TiN_xO_y$(rock-salt) was suppressed by silica-modification, which agrees with the results of XRD. There found some discrepancy between XRD and XPS results: The XRD pattern of $NH_3$-treated XG(0) at 650 °C showed a small diffraction peak due to $TiN_xO_y$(rock-salt), while XPS result did not show any indication of the presence of this phase in the sample. Since the sample was treated in

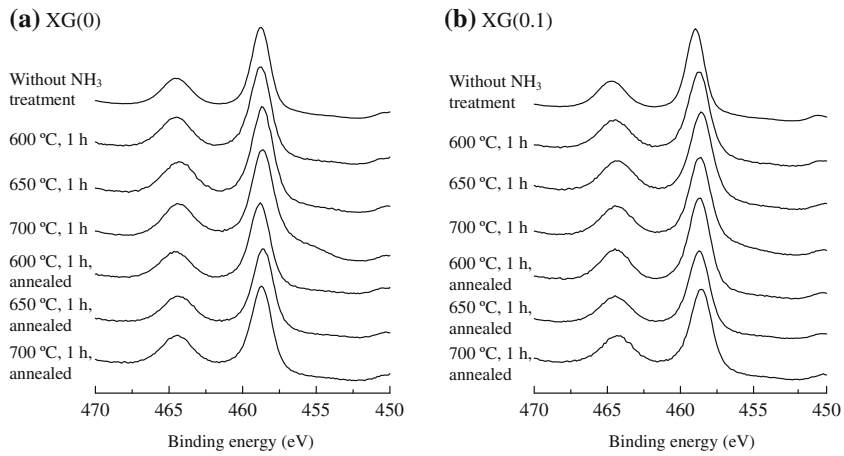


**Fig. 8** Ti 2p XPS spectra of (**a**) XG(0) and (**b**) XG(0.1)

**Table 2** Binding energy of core electrons for nitrified XG(x)'s

| Sample | $NH_3$ treatment | Annealing | $Ti2p_{1/2}$(eV) | $Ti2p_{3/2}$(eV) |
|---|---|---|---|---|
| XG(0) | – | – | 464.5 | 458.8 |
| | 600 °C, 1 h | – | 464.5 | 458.8 |
| | 650 °C, 1 h | – | 464.3 | 458.6 |
| | 700 °C, 1 h | – | 464.4 (81)[a] | 458.6 (82)[a] |
| | | | 461.8 (19) | 456.1 (18) |
| | 600 °C, 1 h | 400 °C, 30 min | 464.5 | 458.8 |
| | 650 °C, 1 h | 400 °C, 30 min | 464.3 | 458.6 |
| | 700 °C, 1 h | 400 °C, 30 min | 464.4 | 458.7 |
| XG(0.1) | – | – | 464.7 | 458.9 |
| | 600 °C, 1 h | – | 464.5 | 458.7 |
| | 650 °C, 1 h | – | 464.3 | 458.6 |
| | 700 °C, 1 h | – | 464.4 (90) | 458.7 (90) |
| | | | 461.7 (10) | 456.2 (10) |
| | 600 °C, 1 h | 400 °C, 30 min | 464.4 | 458.7 |
| | 650 °C, 1 h | 400 °C, 30 min | 464.4 | 458.7 |
| | 700 °C, 1 h | 400 °C, 30 min | 464.3 | 458.6 |

[a] The number in parentheses indicates the percentage of the band

ambient atmosphere before the XRD and XPS measurements, the surface of the sample seems to be oxidized by air. After annealing in air at 400 °C for 30 min, the Ti 2p spectra were quite similar to those for XG(x)'s without the $NH_3$ treatment, which indicates that the $TiN_xO_y$(rock-salt) phase was not included in both XG(0) and XG(0.1). This result also suggests that the proportions of $Ti^{3+}$ in the samples were small although the presence of $Ti^{3+}$ in $NH_3$-treated XG(x)'s with the annealing was indicated by the UV–vis spectra.

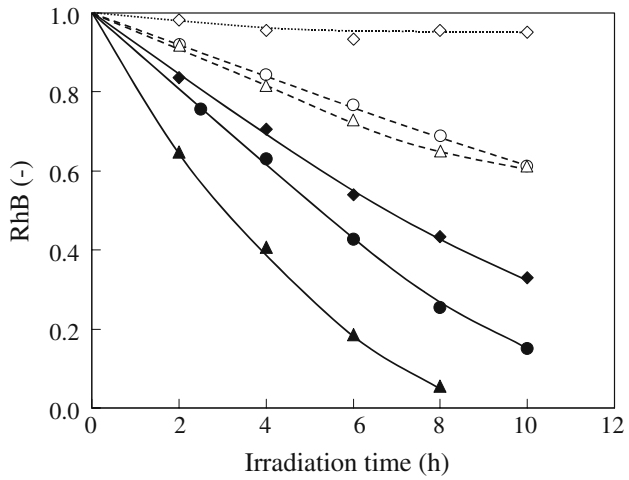


**Fig. 9** Photocatalytic decomposition of RhB under visible light irradiation (◇), without catalyst; (○) and (●), XG(0); (△) and (▲), XG(0.1); (◆), JRC-TIO-4. Open symbols, without the $NH_3$ treatment; solid symbols, after the $NH_3$ treatment at 600 °C for 1 h and annealing at 400 °C in air for 30 min

## Photocatalytic activities of nitrified XG(x)'s

Figure 9 shows the result of photocatalytic degradation of RhB using blue LED as a light source. In this experiment, XG(0) and XG(0.1), both not nitrified, exhibited certain activities; for example, about 30% of RhB was decomposed after irradiation for 10 h. These photocatalytic activities are due to a dye-sensitized photocatalytic reaction, which has been observed in various dye-$TiO_2$ systems [31, 32]. On the other hand, by using the nitrified samples, the decomposition rate increased significantly. Nitrified XG(0.1) obviously showed a higher photocatalytic activity than nitrified XG(0) and JRC-TIO-4.

For $NH_3$-treated XG(0.1) or XG(0) without annealing, the photocatalytic activities were much lower than those of the annealed samples (see Fig. 1 in the supplementary material). This is probably because of the presence of adsorbed $NH_3$ and of the increase in the population of oxygen vacancies, which serve as recombination centers and promote the recombination of holes and electrons [33]. The annealing procedure eliminated the adsorbed $NH_3$ and oxygen vacancies, thus increasing the high photocatalytic activity. However, higher annealing temperature decreases the amount of nitrogen doped and thus reduces the visible light responsibility. Therefore, in this paper, 400 °C was chosen as the annealing temperature.

In order to examine the effect of surface property of the catalysts, zeta potentials of the catalysts were measured and the results are shown in Fig. 10. The isoelectric point of XG(0) was 7.1, while that of XG(0.1) was shifted to the lower pH side, 5.8. Since the isoelectric point of pure $SiO_2$ is ca 2.0, this shift is

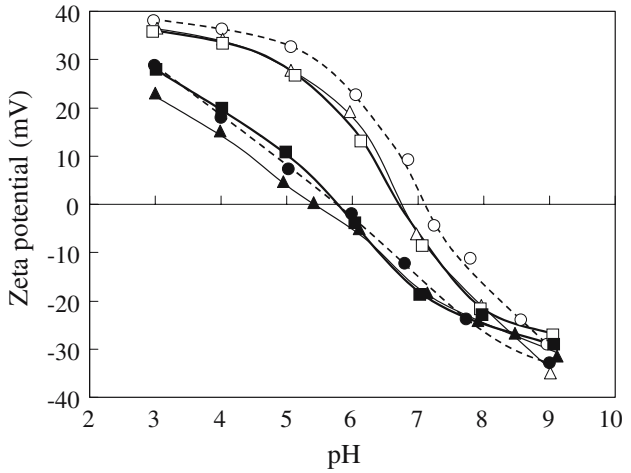


**Fig. 10** Zeta potential as a function of pH: open symbols, for XG(0); closed symbols, for XG(0.1). Circles, without the $NH_3$ treatment; triangles, after the $NH_3$ treatment at 600 °C for 1 h; squares, after the $NH_3$ treatment and annealing at 400 °C in air for 30 min

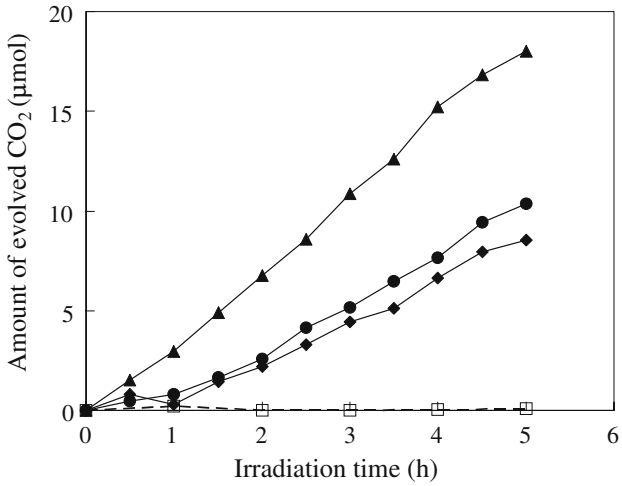


**Fig. 11** Photocatalytic decomposition of acetaldehyde under visible light irradiation: (▲), XG(0.1); (●), XG(0); (♦), JRC-TIO-4; treated in an $NH_3$ flow at 600 °C for 1 h and annealed in air at 400 °C for 30 min, and (□), XG(0)

probably due to a small amount of $SiO_2$ located on the surface of the silica-modified titanias. Such a change in zeta potential, however, did not affect the equilibrium amount of the adsorbed RhB at pH 5 (see Fig. 2 in the supplementary material). Since RhB is a cationic dye, it is preferably adsorbed on the negatively charged surface. In the experiments of RhB photocatalytic decomposition, the pH of the RhB solution was from 4 to 5, and therefore, the surfaces of both XG(0) and XG(0.1) were positively charged. After the $NH_3$ treatment at 600 °C for 1 h and annealing at 400 °C for 30 min, the isoelectric points for both XG(0) and XG(0.1) did not change significantly. These results indicate that the improved photocatalytic activities of the nitrified samples were not because of the change in the surface property. Therefore, we concluded that the improved visible light sensitivity of the nitrified silica-modified titania is due to the increase in the amount of doped nitrogen.

Figure 11 shows the result of photocatalytic decomposition of acetaldehyde on the samples. Under visible light irradiation, evolution of $CO_2$ was not detected for XG(0). On the other hand, using nitrified XG(x)'s, the amount of $CO_2$ increased with the irradiation time, indicating that photocatalytic decomposition of acetaldehyde proceeded under visible light irradiation. Nitrified XG(0.1) obviously showed a higher photocatalytic activity than nitrified XG(0) and JRC-TIO-4. As shown in Fig. 11, the $CO_2$ concentration increased proportionally, suggesting a pseudo-zero-order kinetics with respect to the acetaldehyde concentration (partial pressure). However, induction period was clearly observed for nitrified XG(0) and JRC-TIO-4, indicating presence of intermediates [34–37]. The photocatalytic reaction in this paper was carried out using a relatively weak visible light in the presence of a high concentration of acetaldehyde (0.2 mmol of acetaldehyde in 1 L corresponds to 5,000 ppm) and therefore the $CO_2$ formation rate was not changed when the amount of the acetaldehyde was changed (0.1–0.4 mmol). These results indicate that the reaction rate is not limited by the adsorbability of the reactant on the surface of the catalyst but that the photocatalytic reaction is determined dominantly by the rate of the generation of the photoexcited electron and positive hole as well as the recombination rate of them.

## Conclusions

By the $NH_3$ treatment at a high temperature, both of $TiO_2$ and silica-modified titanias were nitrified. After the $NH_3$ treatment and the annealing in air, the amount of nitrogen introduced to the silica-modified titanias was higher than that of the pure titania. The nitrified silica-modified titanias showed a strong absorption in the visible region (400–500 nm) and exhibited high photocatalytic activities for degradation of RhB and decomposition of acetaldehyde under visible light irradiation.

**Acknowledgements** This study was supported by a Grant-in-Aid for Scientific Research (No. 16510085) from Ministry of Education, Culture, Sports, Science and Technology, Japan, and by the Kansai Research Foundation for Technology Promotion. One of the authors, S. I., thanks Prof. B. Ohtani for valuable discussions.

## References


1. Fujishima A, Rao TN, Tryk DA (2000) J Photochem Photobiol C 1:1
2. Hoffman MR, Martin ST, Choi W, Bahnemann DW (1995) Chem Rev 95:69
3. Serpone N, Lawless D (1994) Langmuir 10:643
4. Anpo M (1997) Catal Surv Jpn 1:169
5. Klosek S, Raftery D (2001) J Phys Chem B 105:2815
6. Sakata Y, Yamamoto T, Okazaki T, Imamura H, Tsuchiya S (1998) Chem Lett 1253
7. Sato S (1986) Chem Phys Lett 123:126
8. Asahi R, Morikawa T, Ohwaki T, Aoki K, Taga Y (2001) Science 293:269
9. Lindgren T, Mwabora JM, Avendaño E, Jonsson J, Hoel A, Granqvist C-G, Lindquist S-E (2003) J Phys Chem B 107:5709
10. Irie H, Watanabe Y, Hashimoto K (2003) J Phys Chem B 107:5483
11. Ohno T, Mitsui T, Matsumura M (2003) Chem Lett 364
12. Luo H, Takata T, Lee Y, Zhao J, Domen K, Yan Y (2004) Chem Mater 16:846
13. Hattori A, Tada H (2001) J Sol–Gel Sci Technol 22:47
14. Iwamoto S, Tanakulrungsank W, Inoue M, Kagawa K, Praserthdam P (2000) J Mater Sci Lett 19:1439
15. Iwamoto Sh, Iwamoto Se, Inoue M, Yoshida H, Tanaka T, Kagawa K (2005) Chem Mater 17:650
16. Ozaki H, Iwamoto S, Inoue M (2005) Chem Lett 34:1082
17. Iwamoto S, Saito K, Inoue M, Kagawa K (2001) Nano Lett 1:417
18. Miyauchi M, Ikezawa A, Tobimatsu H, Irie H, Hashimoto K (2004) Phys Chem Chem Phys 6:865
19. Liu H, Gao L (2004) J Am Ceram Soc 87:1582
20. Sakatani Y, Ando H, Okusako K, Koike H, Nunoshige J, Takata T, Kondo JN, Hara M, Domen K (2004) J Mater Res 19:2100
21. Torimoto T, Fox RJ III, Fox MA (1996) J Electrochem Soc 143:3712
22. Guillot J, Jouaiti A, Imhoff L, Domenichini B, Heintz O, Zerkout S, Mosser A, Bourgeois S (2002) Surf Interface Anal 33:577
23. Makino Y, Nose M, Tanaka T, Misawa M, Tanimoto A, Nakai T, Kato K, Nogi K (1998) Surf Coat Technol 98:934
24. Shinn ND, Tsang KL (1991) J Vac Sci Technol A 9:1558
25. Saha NC, Tompkins HG (1992) J Appl Phys 72:3072
26. Muilenberg GE (1979) In: Handbook of X-ray photoelectron spectroscopy, Perkin-Elmer Corporation, Minnesota, p 40
27. H Höchst, Bringans RD, Steiner P, Wolf TH (1982) Phys Rev B 25:7183
28. Vasile MJ, Emerson AB, Baiocchi FA (1990) J Vac Sci Technol A 8:99
29. Miller AE, Moulder J (1985) J Vac Sci Technol A 3:2415
30. Bertóti I, Mohai M, Sullivan JL, Saied SO (1995) Appl Surf Sci 84:357
31. Wu T, Liu G, Zhao J, Hidaka H, Serpone N (1998) J Phys Chem B 102:5845
32. Vinodgopal K, Kamat PV (1992) J Phys Chem 96:5053
33. Ikeda S, Sugiyama N, Murakami S, Kominami H, Kera Y, Noguchi H, Uosaki K, Torimoto T, Ohtani B (2003) Phys Chem Chem Phys 5:778
34. Sauer ML, Ollis DF (1996) J Catal 158:570
35. Nimlos MR, Wolfrum EJ, Brewer ML, Fennell JA, Bintner G (1996) Environ Sci Technol 30:3102
36. Muggli DS, Lowery KH, Falconer JL (1998) J Catal 180:111
37. Xu J-H, Shiraishi F (1999) J Chem Technol Biotechnol 74:1096